

# A bright radio burst from FRB 20200120E in a globular cluster of the nearby galaxy M81

S. B. Zhang<sup>1\*</sup>, J. S. Wang<sup>2\*</sup>, X. Yang<sup>1,3\*</sup>, Y. Li<sup>1</sup>, J. J. Geng<sup>1</sup>, Z. F. Tang<sup>1,3</sup>, C.M. Chang<sup>1,3</sup>, J. T. Luo<sup>4,5</sup>, X. C. Wang<sup>4</sup>, X. F. Wu<sup>1,3†</sup>, Z. G. Dai<sup>6‡</sup>, B. Zhang<sup>7,8§</sup>

<sup>1</sup>*Purple Mountain Observatory, Chinese Academy of Sciences, Nanjing 210023, China*

<sup>2</sup>*Max-Planck-Institut für Kernphysik, Saupfercheckweg 1, D-69117 Heidelberg, Germany*

<sup>3</sup>*School of Astronomy and Space Sciences, University of Science and Technology of China, Hefei 230026, China*

<sup>4</sup>*National Time Service Center, Chinese Academy of Sciences, Xi'an 710600, China*

<sup>5</sup>*University of Chinese Academy of Sciences, No.19A Yuquan Road, Shijingshan District, Beijing 100049, China*

<sup>6</sup>*Department of Astronomy, University of Science and Technology of China, Hefei 230026, China*

<sup>7</sup>*Nevada Center for Astrophysics, University of Nevada, Las Vegas, NV 89154, USA*

<sup>8</sup>*Department of Physics and Astronomy, University of Nevada, Las Vegas, NV 89154, USA*

**Fast radio bursts (FRBs) are immensely energetic millisecond-duration radio pulses<sup>1,2</sup>. Observations indicate that nearby FRBs can be produced by both young stellar populations, as suggested by the detection of FRB 20200428 from a Galactic magnetar SGR 1935+2154<sup>3,4</sup>, and old stellar populations, as suggested by the localization of the repeating source FRB 20200120E in a globular cluster of M81<sup>5,6</sup>. Nevertheless, the burst energies of FRB 20200120E are significantly smaller than those of other cosmological FRBs<sup>7-9</sup>, even falling below the energy of the Galactic event FRB 20200428<sup>3,4</sup>. Additionally, its burst energy distribution displays a steep power law tail at high fluences<sup>10</sup>. It is unclear whether this type of source can contribute to the cosmological FRB population. Here we report the detection of a burst from FRB 20200120E in 1.1-1.7 GHz, with a fluence of approximately 31.4 Jy ms, which is more than 44 times larger than the previous detected bursts  $\sim 1.4$  GHz frequencies<sup>10,11</sup> and five times more energetic than FRB 20200428<sup>3,4,12</sup>. It reaches one-third of the energy of the weakest burst from FRB 20121102A detected so far<sup>7</sup> and is detectable at a distance exceeding 200 Mpc<sup>13</sup>. This suggests that globular clusters can host cosmological FRBs, and the currently localized FRB sample could contain FRBs from globular clusters. Together with SGR 1935+2154, these two most nearby sources support multiple progenitor sources for FRBs.**

---

\*These authors contributed equally to this work.

†Email: xfwu@pmo.ac.cn

‡Email: daizg@ustc.edu.cn

§Email: zhang@physics.unlv.edu

FRB 20200120E has been identified as a repeating FRB source through the Canadian Hydrogen Intensity Mapping Experiment FRB project (CHIME/FRB)<sup>5</sup>. The European Very Long Baseline Interferometry Network (EVN) then localized it to a globular cluster [PR95] 30244 in the M81 galactic system at a distance of 3.63 Mpc<sup>6</sup>. To search for brighter bursts from FRB 20200120E, we conducted two observing epochs using the 40-meter Haoping radio telescope. Epoch 1 of 22.7 hours spanned September 16 to 17, 2021, while Epoch 2 of 39.8 hours spanned April 13 to 15, 2023. Employing an L-band receiver, we covered a frequency range of 1100 to 1700 MHz. The data were split into three kinds of bands: the full-band (1100–1700 MHz), half-band (1100–1400 MHz and 1400–1700 MHz), and narrow-band (1100–1250 MHz, 1250–1400 MHz, 1400–1550 MHz and 1550–1700 MHz). Two individual search pipelines based on PRESTO<sup>14</sup> and HEIMDALL<sup>15</sup> were employed for data processing. Any candidate with a signal-to-noise ratio (S/N) above seven was recorded and subjected to visual inspection (Methods).

In a total of 62.5 hours, we detected a burst within the Epoch 1 data, which occurred on September 16, 2021, with a barycentric arrival time of 14:37:08.6644 Universal Time (UT) at an infinite frequency. The burst was identified by both PRESTO and HEIMDALL, with S/N of 13.8 and 11.0, respectively, for the full-band data (1100–1700 MHz). In addition, the narrow-band data (1100–1250 MHz) yielded S/N of 29.8 and 28.3 by PRESTO and HEIMDALL, respectively. Figure 1 presents the dynamic spectra and pulse profile of the detected burst, after being de-dispersed using the optimal DM value of 87.82 pc cm<sup>-3</sup>, in general agreement with previous detections<sup>5,10,11,16,17</sup>. The burst has a frequency extent of 1130(4)–1220(4) MHz, an averaged fluence of 31.4±8.6 Jy ms, and a peak flux density of 195±53 Jy (see Table 1).

In previously reported studies, CHIME detected three bursts with fluences from 2.0 to 2.4 Jy ms in the frequency band of 400–800 MHz<sup>5</sup>, Effelsberg recorded 65 bursts with fluences from 0.04 to 0.71 Jy ms within the frequency band of 1200–1600 MHz<sup>6,10</sup>, and DSS-63 observed a burst with a fluence of 0.75±0.15 Jy ms within the frequency band of 2192.5–2307.5 MHz<sup>17</sup>. The burst we detected has a fluence  $\sim$  13 times greater than the brightest burst previously detected. Focusing on the L-band, its fluence is 44–782 times brighter than previous ones. Notably, if positioning FRB 20200120E at a cosmological distance, such as the distance of the nearest localized cosmological FRB 20180916B at 149 Mpc<sup>18</sup>, only this bright “Haoping burst” would be detectable by the Five-hundred-meter Aperture Spherical Radio Telescope (FAST)<sup>13</sup> (Methods). Consequently, the repeating FRB 20200120E would be classified as a nearby apparent one-off FRB if it were placed at a distance of 10s of Mpc. The same could be said for SGR 1935+2154<sup>3,4,16,19,20</sup>.

An energy distribution analysis of the burst sample from the Effelsberg telescope revealed a steep power-law function with an index of  $\sim$  -2.4 at high fluences<sup>10</sup>. According to that function, observations at L-band would be unlikely to detect bursts much exceeding a fluence of 2 Jy ms, which is inconsistent with our detection. Our only detection with S/N $\sim$ 30 and the search threshold of S/N=7 imply a much shallower energy distribution function. This discrepancy might be explained by introducing two distinct energy distributions in different emission states. As a significant number of bursts within the Effelsberg sample were obtained during a 40-minute burst storm, we divided this Effelsberg dataset into two subsets: bursts in the burst storm and bursts

excluding the burst storm. Remarkably, the latter subset displays a relatively flat energy function with the power-law index  $\sim -0.98$ . The detected Haoping burst nicely aligns with the extrapolation of this energy function (Figure 2). Despite being detected at different frequency ranges, it is noteworthy that the bursts recorded by the CHIME and DSS-63 telescopes also align well with the second flatter power-law line. Notably, while the first steep power-law line could also provide a fit for these two samples, our detection significantly deviates from its prediction. Incidentally, a two-component energy function has been identified from other active repeating sources<sup>7</sup>, with FRB 20201124A showing a flatter power-law tail at higher fluences<sup>21</sup>. This suggests that two-component energy function may be a characteristic of repeating FRBs. Noticing that FRB 20201124A is located in a star-forming region<sup>22–25</sup>, the similar energy distribution shape between the two sources hints that this may be an intrinsic behaviour of the central engine regardless of the formation environment.

There are two apparent types of cosmological FRBs: repeaters and apparently one-off bursts (which could be in principle repeaters as well). On the other hand, two nearby events, the Galactic SGR 1935+2154 and FRB 20200120E from M81 offer clues to the engine and formation channels of FRBs: The former points toward a magnetar engine formed from core-collapse supernovae; the latter points toward an unknown engine formed from a certain delayed channel. It is tempting to generalize these two channels to cosmological FRBs. However, these nearby sources are relatively faint compared with their cosmological brethren. FRB 20200428<sup>3,4</sup> was about 1–2 orders of magnitude less luminous than the weakest known extragalactic FRB<sup>7–9</sup>. Many bursts detected from FRB 20200120E, including a burst storm of 53 bursts occurring within 40 minutes<sup>10</sup>, on the other hand, have even smaller energies, with the most intense burst still less energetic than FRB 20200428. As shown in Figure 3, all previously detected bursts from FRB 20200120E fall roughly in the middle between the Crab super-giant pulses<sup>26</sup> and typical repeating FRBs<sup>7,8,18</sup>, making the source as an outlier from cosmological FRBs. One may speculate that the globular cluster channel may not form bright cosmological FRBs, and hence, cannot be the main contributor to the cosmological FRB population. The detection of the Haoping burst instantaneously changed this narrative. Using the distance to the M81 globular cluster [PR95] 30244 of 3.63 Mpc<sup>6</sup>, we derive a specific luminosity of  $3.06 \pm 0.84 \times 10^{30} \text{ erg s}^{-1} \text{ Hz}^{-1}$  and an isotropic-equivalent energy of  $5.79 \pm 1.59 \times 10^{35} \text{ erg}$  for the burst. This energy is about five times greater than the brightest radio burst from SGR 1935+2154<sup>3,12</sup>, and is about 1/3 of the weakest burst of FRB 20121102A<sup>7</sup> (Methods). With the inclusion of this newly detected burst, the energy level of FRB 20200120E essentially reaches the main FRB population (Figure 3). The energy release range of this source now spans up to three orders of magnitude. Our detection indicates that this FRB is not an outlier within the primary FRB population and suggests that globular clusters could serve as a typical environment for cosmological FRBs.

There is compelling evidence that at least some active repeaters track star formation history and therefore originate from prompt formation channels of the FRB engine (likely magnetars)<sup>23–25,27–29</sup>. Our result suggests that at least a fraction of cosmological FRBs may reside in globular clusters and the birth of the engine should have significant delay with respect to star formation. This possibility is supported by the analyses of the DM distribution in the first CHIME FRB catalogue<sup>30</sup>.

With all FRBs in the first catalogue included, a delayed population with respect to star formation history together with the prompt population tracking star formation are needed to reproduce the data<sup>31,32</sup>. Excluding bursts with low DM or low DM excesses with respect to the Galactic contribution, the remaining FRB sample seems to track star formation history well<sup>33</sup>. This further suggests that nearby FRBs likely have a significant contamination from the delayed channel. Indeed, some precisely localized FRBs have similar or even larger offsets from the centre of the host galaxy than FRB 20200120E (Extended Data Figure 1). These bursts could be candidates that reside in globular clusters or have a significant delay with respect to star formation.

The exact engine that powers FRB 20200120E is not identified. The leading model invokes a new-born magnetar formed from mergers of two white dwarfs, two neutron stars, or a white dwarf neutron star pair, or accretion induced collapse of a white dwarf<sup>6,11,34,35</sup>. Before the detection of the Haoping burst, one curious aspect is why a magnetar formed in these channels tend to generate lower-energy bursts than core-collapse formed magnetars. The detection removes such an issue, making it plausible to invoke a universal magnetar engine from multiple formation channels, even though other possibilities are not ruled out (see Methods).

1. Lorimer, D. R., Bailes, M., McLaughlin, M. A., Narkevic, D. J. & Crawford, F. A Bright Millisecond Radio Burst of Extragalactic Origin. *Science* **318**, 777 (2007). 0709.4301.
2. Thornton, D. *et al.* A Population of Fast Radio Bursts at Cosmological Distances. *Science* **341**, 53–56 (2013). 1307.1628.
3. Bochenek, C. D. *et al.* A fast radio burst associated with a Galactic magnetar. *Nature* **587**, 59–62 (2020). 2005.10828.
4. CHIME/FRB Collaboration *et al.* A bright millisecond-duration radio burst from a Galactic magnetar. *Nature* **587**, 54–58 (2020). 2005.10324.
5. Bhardwaj, M. *et al.* A Nearby Repeating Fast Radio Burst in the Direction of M81. *ApJ* **910**, L18 (2021). 2103.01295.
6. Kirsten, F. *et al.* A repeating fast radio burst source in a globular cluster. *Nature* **602**, 585–589 (2022). 2105.11445.
7. Li, D. *et al.* A bimodal burst energy distribution of a repeating fast radio burst source. *Nature* **598**, 267–271 (2021). 2107.08205.
8. Xu, H. *et al.* A fast radio burst source at a complex magnetized site in a barred galaxy. *Nature* **609**, 685–688 (2022). 2111.11764.
9. Marcote, B. *et al.* A repeating fast radio burst source localized to a nearby spiral galaxy. *Nature* **577**, 190–194 (2020). 2001.02222.
10. Nimmo, K. *et al.* A burst storm from the repeating FRB 20200120E in an M81 globular cluster. *MNRAS* **520**, 2281–2305 (2023). 2206.03759.
11. Nimmo, K. *et al.* Burst timescales and luminosities as links between young pulsars and fast radio bursts. *Nature Astronomy* **6**, 393–401 (2022). 2105.11446.
12. Zhou, P. *et al.* Revisiting the Distance, Environment, and Supernova Properties of SNR G57.2+0.8 that Hosts SGR 1935+2154. *ApJ* **905**, 99 (2020). 2005.03517.
13. Jiang, P. *et al.* The fundamental performance of FAST with 19-beam receiver at L band. *Research in Astronomy and Astrophysics* **20**, 064 (2020). 2002.01786.
14. Ransom, S. M. *New search techniques for binary pulsars*. Ph.D. thesis, Harvard University, Massachusetts (2001).
15. Petroff, E. *et al.* A real-time fast radio burst: polarization detection and multiwavelength follow-up. *MNRAS* **447**, 246–255 (2015). 1412.0342.
16. Kirsten, F. *et al.* Detection of two bright radio bursts from magnetar SGR 1935 + 2154. *Nature Astronomy* **5**, 414–422 (2021). 2007.05101.
17. Majid, W. A. *et al.* A Bright Fast Radio Burst from FRB 20200120E with Sub-100 Nanosecond Structure. *ApJ* **919**, L6 (2021). 2105.10987.

18. Chime/Frb Collaboration *et al.* Periodic activity from a fast radio burst source. *Nature* **582**, 351–355 (2020). 2001.10275.
19. Good, D. & Chime/Frb Collaboration. CHIME/FRB Detection of Three More Radio Bursts from SGR 1935+2154. *The Astronomer’s Telegram* **14074**, 1 (2020).
20. Zhu, W. *et al.* A radio pulsar phase from SGR J1935+2154 provides clues to the magnetar FRB mechanism. *arXiv e-prints* arXiv:2307.16124 (2023). 2307.16124.
21. Kirsten, F. *et al.* Connecting repeating and non-repeating fast radio bursts via their energy distributions. *arXiv e-prints* arXiv:2306.15505 (2023). 2306.15505.
22. Ravi, V. *et al.* The host galaxy and persistent radio counterpart of FRB 20201124A. *MNRAS* **513**, 982–990 (2022). 2106.09710.
23. Fong, W.-f. *et al.* Chronicling the Host Galaxy Properties of the Remarkable Repeating FRB 20201124A. *ApJ* **919**, L23 (2021). 2106.11993.
24. Piro, L. *et al.* The fast radio burst FRB 20201124A in a star-forming region: Constraints to the progenitor and multiwavelength counterparts. *A&A* **656**, L15 (2021). 2107.14339.
25. Dong, Y. *et al.* Mapping Obscured Star Formation in the Host Galaxy of FRB 20201124A. *arXiv e-prints* arXiv:2307.06995 (2023). 2307.06995.
26. Bera, A. & Chengalur, J. N. Super-giant pulses from the Crab pulsar: energy distribution and occurrence rate. *MNRAS* **490**, L12–L16 (2019). 1909.13812.
27. Chatterjee, S. *et al.* A direct localization of a fast radio burst and its host. *Nature* **541**, 58–61 (2017). 1701.01098.
28. Tendulkar, S. P. *et al.* The Host Galaxy and Redshift of the Repeating Fast Radio Burst FRB 121102. *ApJ* **834**, L7 (2017). 1701.01100.
29. Niu, C.-H. *et al.* CRAFTS for Fast Radio Bursts: Extending the Dispersion-Fluence Relation with New FRBs Detected by FAST. *ApJ* **909**, L8 (2021). 2102.10546.
30. CHIME/FRB Collaboration *et al.* The First CHIME/FRB Fast Radio Burst Catalog. *ApJS* **257**, 59 (2021). 2106.04352.
31. Zhang, R. C. & Zhang, B. The CHIME Fast Radio Burst Population Does Not Track the Star Formation History of the Universe. *ApJ* **924**, L14 (2022). 2109.07558.
32. Hashimoto, T. *et al.* Energy functions of fast radio bursts derived from the first CHIME/FRB catalogue. *MNRAS* **511**, 1961–1976 (2022). 2201.03574.
33. Shin, K. *et al.* Inferring the Energy and Distance Distributions of Fast Radio Bursts Using the First CHIME/FRB Catalog. *ApJ* **944**, 105 (2023). 2207.14316.

34. Kremer, K., Piro, A. L. & Li, D. Dynamical Formation Channels for Fast Radio Bursts in Globular Clusters. *ApJ* **917**, L11 (2021). 2107.03394.
35. Lu, W., Beniamini, P. & Kumar, P. Implications of a rapidly varying FRB in a globular cluster of M81. *MNRAS* **510**, 1867–1879 (2022). 2107.04059.

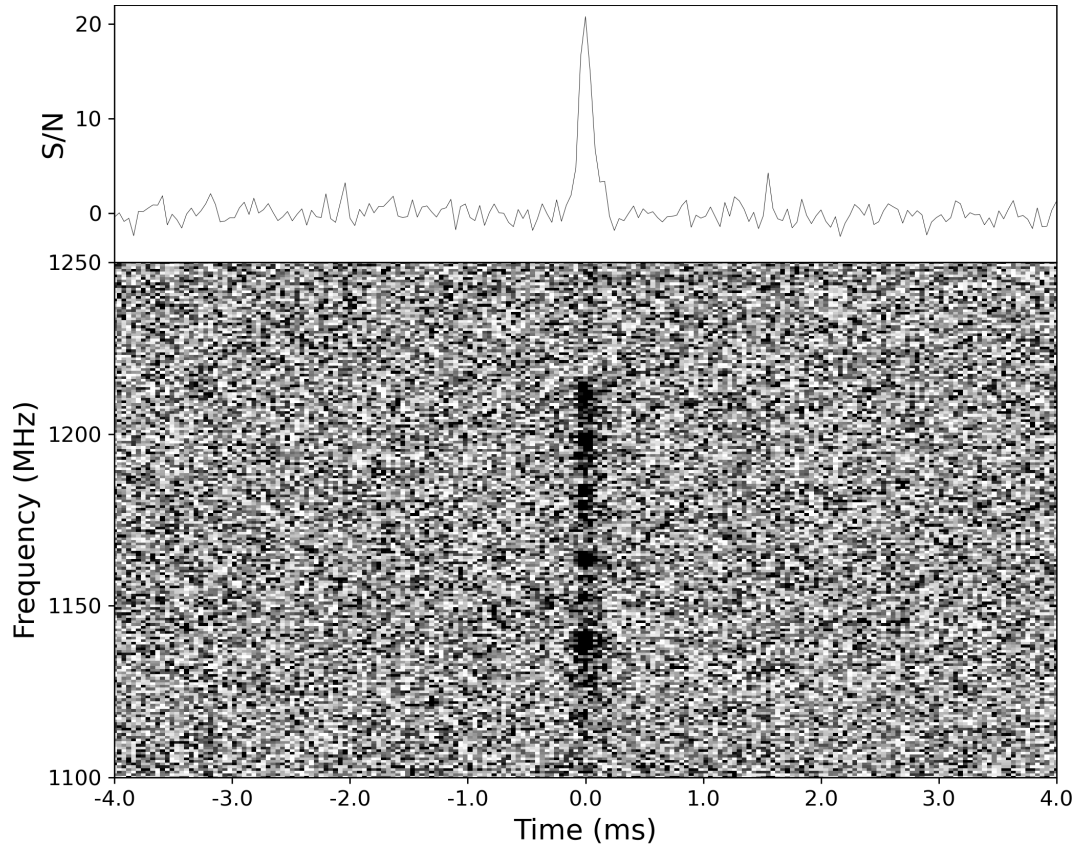


Figure 1: **Integrated pulse profile (top) and dynamic spectra (bottom) of the burst.** The burst is plotted with time and frequency resolutions of  $40.96 \mu\text{s}$  and  $0.78 \text{ MHz}$ , respectively, after being de-dispersed using a DM of  $87.82 \text{ pc cm}^{-3}$ .

Table 1: **The properties of the bright burst from FRB 20200120E.**

<b>Property</b>	<b>Measurement</b>
Time of arrival <sup>a</sup> (MJD)	59473.6091281
DM (pc cm <sup>-3</sup> )	87.82(1) <sup>b</sup>
Width <sup>c</sup> (ms)	0.161(3)
Frequency extent <sup>d</sup> (MHz)	1130(4)–1220(4)
Peak flux density (Jy)	195(53)
Fluence (Jy ms)	31.4(8.6)
Specific luminosity <sup>e</sup> (erg s <sup>-1</sup> Hz <sup>-1</sup> )	3.06(0.84) × 10 <sup>30</sup>
Specific energy release <sup>e</sup> (erg Hz <sup>-1</sup> )	4.93(1.35) × 10 <sup>26</sup>
Isotropic-equivalent energy <sup>f</sup> (erg)	5.79(1.59) × 10 <sup>35</sup>

<sup>a</sup> Corrected to the Solar System Barycentre to infinite frequency assuming a dispersion measure of 87.82 pc cm<sup>-3</sup>.

<sup>b</sup> Determined by maximizing the S/N of the integrated pulse profile.

<sup>c</sup> Effective width.

<sup>d</sup> As the signal is close to the low frequency band edge, we are not sure if signal exists below 1100 MHz.

<sup>e</sup> The specific luminosity/energy release was estimated by scaling the peak flux/fluence by  $4\pi D^2$ , where D is the distance to [PR95] 30244.

<sup>f</sup> To be consistent with the calculations applied to FRB 20200428<sup>3</sup> and FRB 20121102A<sup>7</sup>, the isotropic-equivalent energy was estimated by scaling the specific energy release by  $\nu_0 = 1175$  MHz, which is the midpoint of the burst frequency range (see Methods for different definitions).

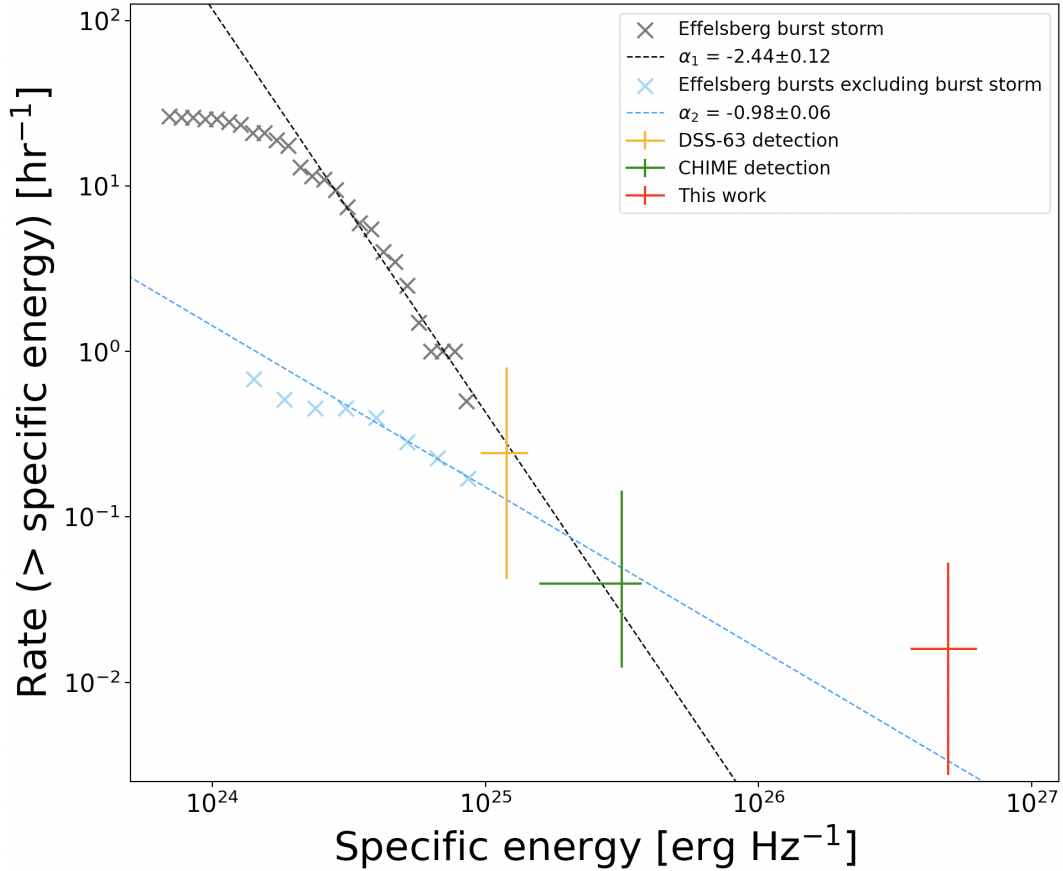


Figure 2: **Distribution of specific energies for bursts originating from FRB 20200120E.** The scatter markers in gray and light blue correspond to the burst storm and other bursts detected by the Effelsberg telescope, respectively. These bursts were fitted with dashed black and blue power law lines for higher fluences, respectively. The orange, green, and red crosses represent bursts with associated errorbars detected by the DSS-63 telescopes, CHIME telescopes, and this work, respectively (see Methods). Notably, the bursts of the CHIME and DSS-63 telescopes were detected at different frequency ranges.

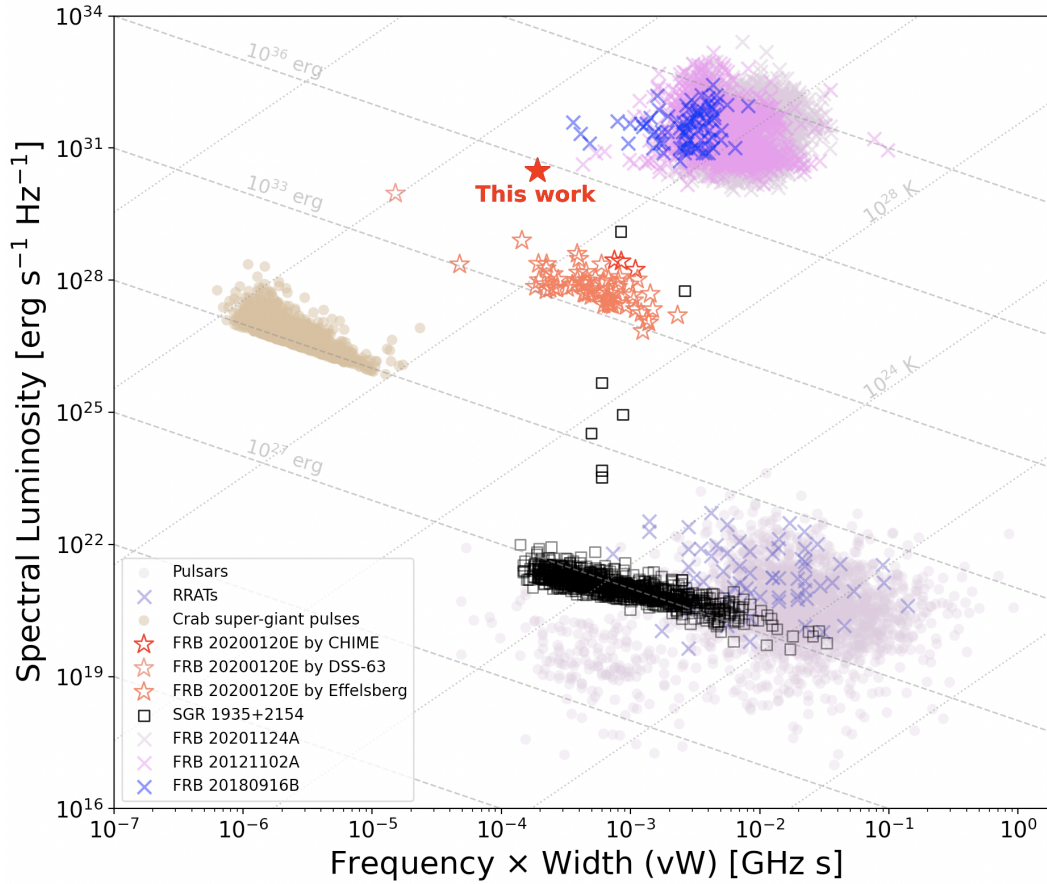


Figure 3: **Isotropic-equivalent spectral luminosity versus frequency  $\times$  width for various coherent radio pulses.** The brightest burst from FRB 20200120E, detected in this study, is denoted by the red filled star. Other bursts from FRB 20200120E, observed by CHIME<sup>5</sup>, DSS-63<sup>17</sup>, and Effelsberg telescopes<sup>6,10</sup>, are represented by the red, salmon, and tomato unfilled stars, respectively. Three well-studied localized repeating FRBs with known distances are also plotted: FRB 20121102A<sup>7</sup> in violet crosses, FRB 20201124A<sup>8</sup> in thistle crosses, and FRB 20180916B<sup>18,36,37</sup> in blue crosses. Radio bursts or pulses from the Galactic magnetar SGR 1935+2154<sup>3,4,16,19,20</sup> are denoted by black squares, while super-giant pulses from the Crab pulsar<sup>26</sup> are shown in tan. The pulsar<sup>38</sup> and rotating radio transient (RRAT) population (RRATalog) are marked in thistle and slateblue, respectively. The grey dashed lines denote constant isotropic-equivalent energy release, with no clear gap existing between various radio pulses. The grey dotted lines represent constant brightness temperature. The x-axis represents transient width, multiplied by the central observing frequency.

## Methods

### Observations and burst detection

Observations for this study were carried out using the 40 m–diameter Haoping radio telescope, which consists of two epochs: Epoch 1 from September 16 to 17, 2021, lasting 22.7 hours, and Epoch 2 from April 13 to 15, 2023, spanning 39.8 hours. The receiver was within the L-band, covering a frequency range of 1100 to 1700 MHz. The single-polarization signals were 8-bit sampled and channelized using the Reconfigurable Open Architecture Computing Hardware generation 2 (ROACH 2)<sup>39</sup>. Subsequently, the data were stored in the PSRFITS search mode format<sup>40</sup>. The specific sample time and channel width for Epoch 1’s observation were set at 40.96  $\mu\text{s}$  and 0.195 MHz, respectively. Due to the site’s observation constraints during Epoch 2, the sample time was 81.92  $\mu\text{s}$ , and the channel width was 0.390 MHz. To verify the observation setup and search pipelines, a bright pulsar PSR J0332+5434 has been observed prior to each FRB 20200120E observation.

The data collected from the Haoping radio telescope were processed to create three different kinds of band datasets for search: the full-band (1100–1700 MHz), half-band (1100–1400 MHz and 1400–1700 MHz) and narrow-band (1100–1250 MHz, 1250–1400 MHz, 1400–1550 MHz and 1550–1700 MHz). These datasets were analyzed via two individual search pipelines, based on the pulsar/FRB single pulse searching packages PRESTO<sup>14</sup> and HEIMDALL<sup>15</sup>. The datasets were dedispersed in a range of DM values from 78 to 98  $\text{cm}^{-3}$  pc, with a step size of 0.01  $\text{cm}^{-3}$ .

Any candidate with a S/N greater than seven was recorded and subject to visual inspection. Within the 62.5 hours of observation, a burst was detected in the data from Epoch 1, occurring on September 16, 2021, with a barycentric arrival time of 14:37:8.6644 Universal Time (UT) at an infinite frequency. Both PRESTO and HEIMDALL successfully indentified this burst, yielding S/N of 13.8 and 11.0 for the full-band data (1100–1700 MHz), S/N of 22.5 and 18.8 for the half-band data (1100–1400 MHz), and S/N of 29.8 and 28.3 for the narrow-band data (1100–1250 MHz), respectively.

### Estimation of flux, fluence, and energy of the burst

To estimate the burst’s flux densities, we employed two methods:

**(1) Radiometer equation approach:** We refer to the radiometer equation:

$$S_{lim} = \frac{S/N T_{sys}}{G \sqrt{\Delta\nu N_p t_{obs}}}, \quad (1)$$

where we ignore the loss factor owing to the 8-bit sampling,  $S/N = 24.7$  is the burst S/N at the specified time resolution and frequency range of  $t_{obs} = 40.96 \mu\text{s}$  and 1130–1220 MHz ( $\Delta\nu = 90$  MHz),  $T_{sys} \sim 100\text{K}$  is the system temperature,  $G \sim 0.23\text{K/Jy}$  is the telescope antenna gain<sup>41</sup>,

and  $N_p = 1$  as only the right-handed single-polarization was employed. This computation yielded an estimated peak flux of  $177 \pm 35$  Jy, accounting for a 20% uncertainty in system temperature fluctuation.

**(2) Comparison to pulsar PSR J0332+5434:** We also examined data from the pulsar PSR J0332+5434 prior to Epoch 1. Opting for a 30-minute observation minimally affected by radio interference (RFI), we folded the pulsar data using the DSPSR<sup>42</sup> and PSRCHIVE<sup>43</sup> packages, based on its time ephemeris<sup>44</sup>. Utilizing the mean flux density at 1400 MHz and the period of PSR J0332+5434<sup>45</sup>, we scaled the fluence of our burst data to Jy ms units. This approach resulted in a fluence of  $31.4 \pm 0.84$  Jy ms (corresponding to peak flux of  $195 \pm 53$  Jy), accounting for a 27% uncertainty related to the mean flux density measurement of the pulsar.

Notably, the flux estimations attained from both methods exhibit congruence. For the main text, we adopted the value derived from the second approach due to the unavailability of precise gain and system temperature measurements for the Haoping telescope. To compute the fluence, we integrated the burst flux above the baseline, while the effective width was determined by dividing the fluence by the burst peak flux. If positioning this burst at the distance of the nearest other extragalactic repeating FRB, FRB 20180916B at 149 Mpc, it would exhibit a peak flux of approximately 115 mJy. The FAST telescope has a system temperature of  $\sim 20$  K and a gain of  $16 \text{ K/Jy}^{13}$ . Taking into account  $N_p = 2$  and  $t_{\text{obs}}$  using the burst width, the sensitivity of this high-sensitive instrument at L-band could yield  $16\sigma$  detection. Additionally, when considering the gain and system temperature for CHIME and the Parkes cryoPAF, which are  $1.16 \text{ K/Jy}$  and  $50 \text{ K}^{46}$ , and  $0.735 \text{ K/Jy}$  and  $20 \text{ K}^{47}$ , respectively, these two instruments could obtain  $7\sigma$  detection for such a burst at distances of approximate 38 Mpc and 48 Mpc, respectively.

### Bursts of FRB 20200120E from different telescopes

In previous studies, burst detections from FRB 20200120E have been reported by three telescopes. According to the CHIME real-time FRB report, eight candidate bursts from this source were identified within the frequency range of 400–800 MHz, yet the properties of only three of them are available<sup>5</sup>. These three bursts were detected from January 20 to November 29, 2020, corresponding to an expected on-source time of about 41 hours<sup>30</sup>. However, the on-source exposure would increase to about 111 hours if one uses the starting date of the CHIME FRB project on July 25, 2018. We employed the properties and expected exposure time of these three bursts to estimate the event rate of CHIME detections<sup>48</sup>. The Effelsberg telescope recorded a total of 65 bursts, with fluences ranging from 0.04–0.71 Jy ms within the frequency band of 1200–1600 MHz<sup>6,10</sup>. The DSS-63 telescope identified a burst with a fluence of  $0.75 \pm 0.15$  Jy ms within the frequency band of 2192.5–2307.5 MHz<sup>17</sup>.

## Luminosities and burst durations for various coherent radio pulses.

To ensure consistency with previous investigations of various coherent radio pulses<sup>11,49</sup>, we presented diverse coherent radio pulses in a two-dimensional plane in Figure 3. The horizontal axis represents the transient width multiplied by the central observing frequency, while the vertical axis depicts the isotropic-equivalent spectral luminosity. The burst detected in this study was present using the central burst frequency. The primary focus of this study is energy release, we omitted the results from the detailed burst temporal structures and applied the effective width or the width of the pulse at 50% of its peak ( $W_{50}$ ) of the whole event as the burst duration. Within Figure 3, we also introduced constant lines denoting the isotropic-equivalent energy release and brightness temperature.

The datasets of radio pulses in this research are follows: (1) other bursts from FRB 20200120E, observed by CHIME<sup>5</sup>, DSS-63<sup>17</sup>, and Effelsberg telescopes<sup>6,10</sup>; (2) three well-studied localized repeating FRBs: FRB 20121102A<sup>7</sup>, FRB 20201124A<sup>8</sup> and FRB 20180916B<sup>18,36,37</sup>; (3) radio bursts or pulses from the Galactic magnetar SGR 1935+2154<sup>3,4,16,19,20</sup> using a distance of 6.6 kpc; (4) a sample of super-giant pulses from the Crab pulsar<sup>26</sup>; (5) single pulses of RRATs (RRATalog), and (6) pulsars at 1400 MHz<sup>38</sup>. For pulsars and RRATs, we presented the average properties of pulses from these sources. It's noteworthy that individual pulses could vary in terms of brightness and duration, typically by approximately 1 order of magnitude, with some deviations even reaching up to 3 orders of magnitude<sup>50</sup>. The luminosities of phenomena in (1) to (5) were estimated through peak flux density. However, for (6) pulsars, luminosities were calculated using the mean flux density averaged over the pulsar period ( $P_0$ )<sup>51</sup>. Throughout this study, we modified the pulsar luminosities to isotropic-equivalent spectral luminosity by multiplying them by the ratio of  $P_0$  to  $W_{50}$ .

## Estimation and comparison of isotropic-equivalent energy

Three methods could be used to compare the energies of different radio pulses: (1) the specific isotropic-equivalent energy:

$$E_S = \frac{4\pi D_L^2}{1+z} F, \quad (2)$$

where  $D_L$  is the luminosity distance,  $z$  is the redshift, and  $F$  is the pulse fluence. (2) the isotropic-equivalent energy by scaling  $E_S$  by central frequency ( $E_{cf}$ ), and (3) isotropic-equivalent energy by scaling  $E_S$  by burst frequency extent ( $E_{fe}$ ).

As our primary comparisons involve our burst, FRB 20200428<sup>3</sup> and FRB 20121102A<sup>7</sup>, in the main text, we used (2) to be consistent with their calculations. The estimated energy of our burst, FRB 20200428 and the weakest burst of FRB 20121102A are  $\sim 5.8 \times 10^{35}$ ,  $1.1 \times 10^{35}$ , and  $1.7 \times 10^{36}$  erg, respectively. Applying (1), the estimated specific energy of these three events are  $\sim 4.9 \times 10^{26}$ ,  $8.0 \times 10^{25}$ , and  $1.3 \times 10^{27}$  erg Hz<sup>-1</sup>, respectively. Applying (3) the estimated energy of these three events are  $\sim 4.4 \times 10^{34}$ ,  $1.5 \times 10^{34}$ , and  $1.4 \times 10^{35}$  erg, respectively.

## Comparison of the FRB 20200120E environment with other FRBs

The environments of transients usually reveal the population of the progenitors. In general, progenitors from young populations reside in the central bright region of the host galaxies, with small offsets from the galaxy centres, while those from old populations are in the outer faint region of the host galaxies and have large offsets<sup>52,53</sup>. FRB 20200120E is located in the edge of the host galaxy, with a large offset of  $20_{-2}^{+3}$  kpc<sup>5</sup>, consistent with a globular cluster origin.

In order to examine whether other FRBs are consistent with a globular cluster origin, we examine the normalized offsets of them with respect to the host galaxy centers based on the available data<sup>54,55</sup>. In addition, for FRBs that lack host galaxy radius or offset information, we searched for the host galaxy information with the FRB positions in the SDSS, DESI/Legacy Survey as well as Pan-STARRS catalog, and estimate the offset with the FRB and host galaxy position. The results are presented in Extended Data Figure 1, which show that a fraction of cosmological FRBs indeed have a normalized offset similar to or larger than that of FRB 20200120E.

## Implications for FRB engine models

The observational properties of FRBs (short duration, high brightness temperature, strong linear polarization, etc) have propelled theories involving compact stars, especially neutron stars, as potential sources<sup>57</sup>. These theories encompass scenarios involving highly magnetized neutron stars or magnetars<sup>58–65</sup>, young Crab-like pulsars<sup>66</sup>, or various interacting neutron stars in binary systems<sup>67–70</sup> or with small bodies<sup>71,72</sup>. The fact that the Haoping burst carries an energy level exceeding FRB 20200428 from SGR 1935+2154 and comparable with faintest cosmological FRBs raised the perspective of interpreting all FRBs with a unified magnetar engine. Nonetheless, in terms of energetics, several other scenarios are still allowed besides the magnetar model. In the following, we discuss various models in turn.

### 1. The magnetar models

For the magnetar models, the energy of the bursts mainly come from the dissipation of internal magnetic energy. For a typical magnetar with an internal field  $B_* = 10^{14} B_{14}$  G and a canonical radius  $R_{\text{NS}} = 10^6$  cm, the internal magnetic energy is  $E_B = 1.67 \times B_{14}^2 10^{45}$  erg. The average energy dissipation rate is

$$\dot{E}_B = E_B/t_{\text{amb}} = 5.6 \times 10^{32} B_{14}^{3.2} \text{ erg/s}, \quad (3)$$

where the dissipation time due to ambipolar diffusion is  $t_{\text{amb}} = 2 \times 10^5 B_{14}^{-1.2} \text{ yr}$ <sup>73</sup>. The average isotropic equivalent luminosity of this event over our observation time is  $\bar{L} = 5.79 \times 10^{35} \text{ erg}/62.5 \text{ h} = 2.6 \times 10^{30} \text{ erg/s}$ <sup>34,35</sup>. Assuming a radiation efficiency  $f_r = 10^{-5} f_{r,-5}$  of the FRB event<sup>3,74</sup>, the magnetar producing FRB 20200120E should have an internal magnetic field  $B_{14} \approx 6.7 f_{r,-5}^{-0.31}$  and a corresponding dissipation time  $t_{\text{amb}} = 9.4 \times 10^3 f_{r,-5}^{-0.375} \text{ yr}$ . This suggests that a young magnetar is enough to power this source.

## 2. Young pulsar giant pulse models

The giant pulse like model assumes that FRBs are powered by the spin-down of NSs<sup>66</sup>. For a canonical NS with moment of inertia  $I_{\text{NS}} \approx 10^{45} \text{ g cm}^2$ , the spin-down luminosity due to magnetic dipole radiation is

$$L_{\text{sd}} = 4.8 \times 10^{42} B_{12}^2 P_{-3}^{-4} (1 + t/\tau_{\text{sd}})^{-2} \text{ erg/s}, \quad (4)$$

where  $\tau_{\text{sd}} = 130 P_{-3}^2 B_{12}^{-2} \text{ yr}$  is the spin-down time scale of an NS with surface magnetic field  $B = 10^{12} B_{12} \text{ G}$  and initial period  $P = 10^{-3} P_{-3} \text{ s}$ . It can be seen that for  $t < \tau_{\text{sd}}$ , the luminosity remains almost constant, otherwise it will decrease as  $L_{\text{sd}} \propto t^{-2}$ . As this FRB is still active, we mainly consider the case of for  $t < \tau_{\text{sd}}$ . The peak luminosity of this event is  $L_p = 3.6 \times 10^{39} \text{ erg/s}$ . Taking a radiation efficiency of giant pulses at  $f_r = 10^{-1} f_{r,-1}$ <sup>66</sup>, we found that the NS needs to have an initial period  $P_{-3} \lesssim 2.3 B_{12}^{1/2} f_{r,-2}^{1/4}$  and a corresponding spin down time of  $\tau_{\text{sd}} \lesssim 686 B_{12}^{-1} f_{r,-2}^{1/2} \text{ yr}$ . Recycled pulsars in globular clusters can have millisecond periods<sup>75</sup>, but with a weak surface magnetic field ( $\lesssim 10^{10} \text{ G}$ )<sup>38</sup>. Therefore, recycled pulsars can not power such event, and a young NS is required. However, the possibility of associating with pulsar wind nebulae has been disfavored from X-ray observation<sup>76</sup>.

## 3. Interacting neutron star models

There are in general two types of magnetosphere interaction models form NS binaries: NS-NS inspiral model<sup>67-70</sup> and NS-asteroid interaction model<sup>71,72</sup>. For the NS-asteroid interaction model, the NS may have a main-sequence star companion, which hosts an asteroid belt. The NS may interact with the asteroids and produces FRBs. The FRB energy mainly comes from the gravitational potential of the planet, which is

$$E = 1.9 \times 10^{38} m_{18} \text{ erg}, \quad (5)$$

for a planet with mass  $m = 10^{18} m_{18} \text{ g}$ <sup>72</sup>. For the observed event with energy  $8.70 \times 10^{32} - 5.79 \times 10^{35} \text{ erg}$ <sup>11</sup>, this requires asteroids to be  $4.7 \times 10^{12} - 3.1 \times 10^{15} \text{ g}$ .

The NS-NS spiral model is usually supposed to be responsible for non-repeating FRBs, as it can produce a luminous event during the last orbits. But it also works when the NSs are widely separated, although the luminosity will become much lower. For two NSs with equal surface magnetic field and anti-parallel magnetic axes, the electromagnetic luminosity from magnetosphere interaction is

$$L_{\text{inspiral}} = 3.4 \times 10^{39} B_{12}^2 a_9^{-2} \text{ erg/s}, \quad (6)$$

at a separation of  $a = 10^9 a_9 \text{ cm}$ <sup>68</sup>. While the merger time for NSs with mass  $M = 1.4 M_{\odot}$  is  $t_{\text{merger}} = 3.2 a_9^4 \text{ yr}$  for binaries with separation  $a \gg R_{\text{NS}}$ <sup>77</sup>. Again assuming the radiation efficiency of giant pulses, the requirement on the surface magnetic field of both NSs is  $B_{12} = 3.2 a_9 f_{r,-1}^{-1/2}$ . Therefore, in principle, NS-NS inspiral cannot be excluded for this event, which could be potentially serve as a new type of electromagnetic counterparts of gravitational wave events.

## References

36. Pleunis, Z. *et al.* LOFAR Detection of 110-188 MHz Emission and Frequency-dependent Activity from FRB 20180916B. *ApJ* **911**, L3 (2021). 2012.08372.
37. Nimmo, K. *et al.* Highly polarized microstructure from the repeating FRB 20180916B. *Nature Astronomy* **5**, 594–603 (2021). 2010.05800.
38. Manchester, R. N., Hobbs, G. B., Teoh, A. & Hobbs, M. The Australia Telescope National Facility Pulsar Catalogue. *AJ* **129**, 1993–2006 (2005). astro-ph/0412641.
39. Hickish, J. *et al.* A Decade of Developing Radio-Astronomy Instrumentation using CASPER Open-Source Technology. *Journal of Astronomical Instrumentation* **5**, 1641001–12 (2016). 1611.01826.
40. Hotan, A. W., van Straten, W. & Manchester, R. N. PSRCHIVE and PSRFITS: An Open Approach to Radio Pulsar Data Storage and Analysis. *Publications of the Astronomical Society of Australia* **21**, 302–309 (2004). astro-ph/0404549.
41. Men, Y. P. *et al.* Piggyback search for fast radio bursts using Nanshan 26 m and Kunming 40 m radio telescopes - I. Observing and data analysis systems, discovery of a mysterious peryton. *MNRAS* **488**, 3957–3971 (2019). 1907.13056.
42. van Straten, W. & Bailes, M. DSPSR: Digital Signal Processing Software for Pulsar Astronomy. *Publications of the Astronomical Society of Australia* **28**, 1–14 (2011). 1008.3973.
43. van Straten, W., Demorest, P. & Osłowski, S. Pulsar Data Analysis with PSRCHIVE. *Astronomical Research and Technology* **9**, 237–256 (2012). 1205.6276.
44. Hobbs, G., Lyne, A. G., Kramer, M., Martin, C. E. & Jordan, C. Long-term timing observations of 374 pulsars. *MNRAS* **353**, 1311–1344 (2004).
45. Lorimer, D. R., Yates, J. A., Lyne, A. G. & Gould, D. M. Multifrequency flux density measurements of 280 pulsars. *MNRAS* **273**, 411–421 (1995).
46. CHIME/FRB Collaboration *et al.* Observations of fast radio bursts at frequencies down to 400 megahertz. *Nature* **566**, 230–234 (2019). 1901.04524.
47. Manchester, R. N. *et al.* The Parkes multi-beam pulsar survey - I. Observing and data analysis systems, discovery and timing of 100 pulsars. *MNRAS* **328**, 17–35 (2001). astro-ph/0106522.
48. Gehrels, N. Confidence Limits for Small Numbers of Events in Astrophysical Data. *ApJ* **303**, 336 (1986).
49. Bailes, M. The discovery and scientific potential of fast radio bursts. *Science* **378**, abj3043 (2022). 2211.06048.

50. Zhang, S. B. *et al.* RRAT J1913+1330: an extremely variable and puzzling pulsar. *arXiv e-prints* arXiv:2306.02855 (2023). 2306.02855.
51. Lorimer, D. R. & Kramer, M. *Handbook of Pulsar Astronomy* (2012).
52. Bloom, J. S., Kulkarni, S. R. & Djorgovski, S. G. The Observed Offset Distribution of Gamma-Ray Bursts from Their Host Galaxies: A Robust Clue to the Nature of the Progenitors. *AJ* **123**, 1111–1148 (2002). astro-ph/0010176.
53. Fong, W. & Berger, E. The Locations of Short Gamma-Ray Bursts as Evidence for Compact Object Binary Progenitors. *ApJ* **776**, 18 (2013). 1307.0819.
54. Bhandari, S. *et al.* Characterizing the Fast Radio Burst Host Galaxy Population and its Connection to Transients in the Local and Extragalactic Universe. *AJ* **163**, 69 (2022). 2108.01282.
55. Law, C. J. *et al.* Deep Synoptic Array Science: First FRB and Host Galaxy Catalog. *arXiv e-prints* arXiv:2307.03344 (2023). 2307.03344.
56. Ravi, V. *et al.* Deep Synoptic Array Science: Discovery of the Host Galaxy of FRB 20220912A. *ApJ* **949**, L3 (2023). 2211.09049.
57. Zhang, B. The physics of fast radio bursts. *Reviews of Modern Physics* **95**, 035005 (2023). 2212.03972.
58. Popov, S. B. & Postnov, K. A. Hyperflares of SGRs as an engine for millisecond extragalactic radio bursts. In Harutyunian, H. A., Mickaelian, A. M. & Terzian, Y. (eds.) *Evolution of Cosmic Objects through their Physical Activity*, 129–132 (2010). 0710.2006.
59. Katz, J. I. Inferences from the Distributions of Fast Radio Burst Pulse Widths, Dispersion Measures, and Fluences. *ApJ* **818**, 19 (2016). 1505.06220.
60. Metzger, B. D., Berger, E. & Margalit, B. Millisecond Magnetar Birth Connects FRB 121102 to Superluminous Supernovae and Long-duration Gamma-Ray Bursts. *ApJ* **841**, 14 (2017). 1701.02370.
61. Beloborodov, A. M. A Flaring Magnetar in FRB 121102? *ApJ* **843**, L26 (2017). 1702.08644.
62. Kumar, P., Lu, W. & Bhattacharya, M. Fast radio burst source properties and curvature radiation model. *MNRAS* **468**, 2726–2739 (2017). 1703.06139.
63. Yang, Y.-P. & Zhang, B. Bunching Coherent Curvature Radiation in Three-dimensional Magnetic Field Geometry: Application to Pulsars and Fast Radio Bursts. *ApJ* **868**, 31 (2018). 1712.02702.
64. Lu, W., Kumar, P. & Zhang, B. A unified picture of Galactic and cosmological fast radio bursts. *MNRAS* **498**, 1397–1405 (2020). 2005.06736.

65. Margalit, B., Beniamini, P., Sridhar, N. & Metzger, B. D. Implications of a Fast Radio Burst from a Galactic Magnetar. *ApJ* **899**, L27 (2020). 2005.05283.
66. Cordes, J. M. & Wasserman, I. Supergiant pulses from extragalactic neutron stars. *MNRAS* **457**, 232–257 (2016). 1501.00753.
67. Wang, J.-S., Yang, Y.-P., Wu, X.-F., Dai, Z.-G. & Wang, F.-Y. Fast Radio Bursts from the Inspiral of Double Neutron Stars. *ApJ* **822**, L7 (2016). 1603.02014.
68. Wang, J.-S., Peng, F.-K., Wu, K. & Dai, Z.-G. Pre-merger Electromagnetic Counterparts of Binary Compact Stars. *ApJ* **868**, 19 (2018). 1810.00170.
69. Zhang, B. Charged Compact Binary Coalescence Signal and Electromagnetic Counterpart of Plunging Black Hole-Neutron Star Mergers. *ApJ* **873**, L9 (2019). 1901.11177.
70. Zhang, B. Fast Radio Bursts from Interacting Binary Neutron Star Systems. *ApJ* **890**, L24 (2020). 2002.00335.
71. Geng, J. J. & Huang, Y. F. Fast Radio Bursts: Collisions between Neutron Stars and Asteroids/Comets. *ApJ* **809**, 24 (2015). 1502.05171.
72. Dai, Z. G., Wang, J. S., Wu, X. F. & Huang, Y. F. Repeating Fast Radio Bursts from Highly Magnetized Pulsars Traveling through Asteroid Belts. *ApJ* **829**, 27 (2016). 1603.08207.
73. Beloborodov, A. M. & Li, X. Magnetar Heating. *ApJ* **833**, 261 (2016). 1605.09077.
74. Li, C. K. *et al.* HXMT identification of a non-thermal X-ray burst from SGR J1935+2154 and with FRB 200428. *Nature Astronomy* **5**, 378–384 (2021). 2005.11071.
75. Verbunt, F. & Lewin, W. H. G. Globular cluster X-ray sources. In *Compact stellar X-ray sources*, vol. 39, 341–379 (2006).
76. Pearlman, A. B. *et al.* Multiwavelength Constraints on the Origin of a Nearby Repeating Fast Radio Burst Source in a Globular Cluster. *arXiv e-prints* arXiv:2308.10930 (2023). 2308.10930.
77. Peters, P. C. Gravitational Radiation and the Motion of Two Point Masses. *Physical Review* **136**, 1224–1232 (1964).

## Data availability

RRATALOG (<https://rratalog.github.io/rratalog/>)

Data are available upon request. These data are in a public archive at [https://github.com/Astroyx/M81\\_FRB\\_haoping](https://github.com/Astroyx/M81_FRB_haoping)

## Code availability

PRESTO (<http://www.cv.nrao.edu/~sransom/presto/>)

HEMIDALL (<https://sourceforge.net/projects/heimdall-astro/>)

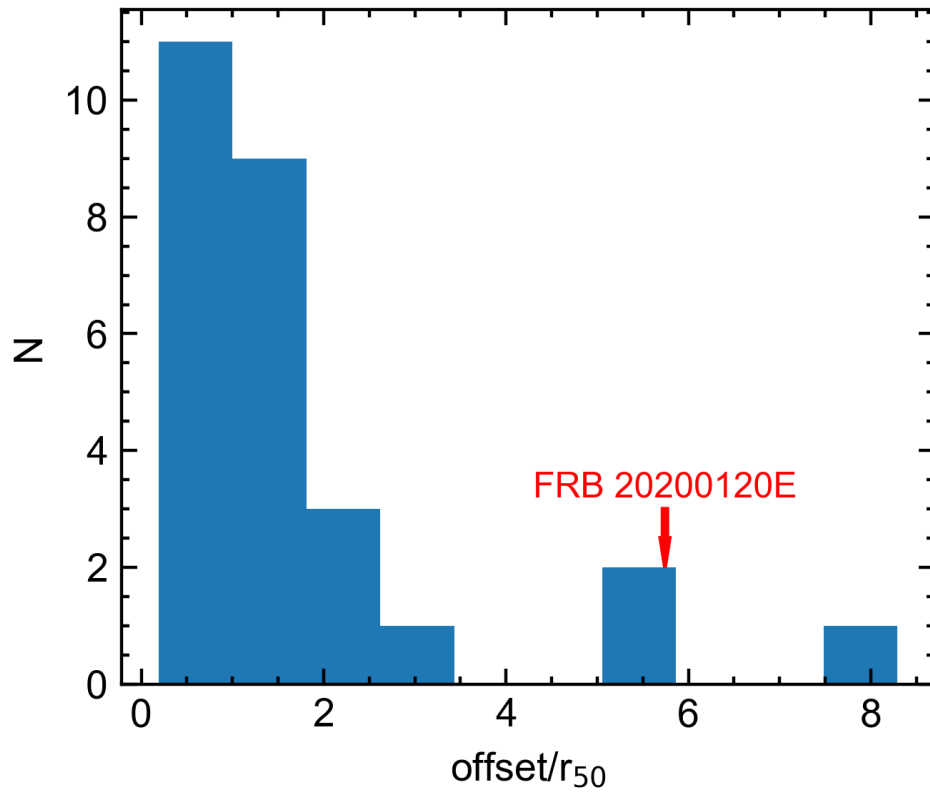
PSRCHIVE (<http://psrchive.sourceforge.net>)

**Acknowledgements** We thank Apurba Bera for the Crab data. This work is partially supported by the National Key Research and Development Program of China (2022SKA0130100,2020SKA0120300), the National Natural Science Foundation of China (grant Nos. 12041306, 12273113,12233002,12003028,12321003), the international Partnership Program of Chinese Academy of Sciences for Grand Challenges (114332KYSB20210018), the National Key R&D Program of China (2021YFA0718500), the ACAMAR Postdoctoral Fellow, China Postdoctoral Science Foundation (grant No. 2020M681758), and the Natural Science Foundation of Jiangsu Province (grant Nos. BK20210998). JJG acknowledges the support from the Youth Innovation Promotion Association (2023331). JSW acknowledges the support from the Alexander von Humboldt Foundation.

**Author Contributions** SBZ, JSW and XFW launched the Haoping observation of FRB 20200120E; SBZ, XY, ZFT, CMC, JTL and XCW carried out the observation and processed the data; BZ, ZGD, JSW, YL and JJG analysed the results and discussed the theoretical models. All authors contributed to the analysis or interpretation of the data and to the final version of the manuscript.

**Competing Interests** The authors declare that they have no competing financial interests.

**Correspondence** Correspondence and requests for materials should be addressed to X. F. Wu, Z. G. Dai or B. Zhang.



**Extended Data Figure 1: Offsets of FRBs.** The offset of 27 FRBs from the centre of the host galaxies, normalized to the half light radii  $r_{50}$  of the hosts. One can see that 3 FRBs have a normalized offset comparable to or larger than that of FRB 20200120E.